

# E15 first-stage status and a second-stage request

*submitted on May 7, 2014*

E15 collaboration

## Abstract

We report a summary of the E15 data analysis based on the first-stage physics run and a beam-time request for the second-stage. The first physics data-taking was carried out in March and May, 2013 with  $6 \times 10^9$  kaons on  ${}^3\text{He}$  target corresponding to  $\sim 1\%$  of the approved proposal. By analysing semi-inclusive  ${}^3\text{He}(K^-, n)$  and exclusive  ${}^3\text{He}(K^-, \Lambda p)n$  channels, a significant excess around the  $\bar{K}NN$  threshold was observed both in the neutron missing-mass and in the  $\Lambda p$  invariant-mass spectra. To investigate whether or not the excess is related with any nuclear exotic state, such as a kaonic bound state  $K^-pp$ , we need high statistics data-taking. We wish to make the next step with 10 times more integrated beam-kaons than that of the first-stage in May, 2013.

## Summary of the second-stage experiment:

Beamline: K1.8BR  
Secondary beam: 1.0 GeV/c  $K^-$   
Beam intensity: more than  $1.4 \times 10^5$  per spill (6 s repetition rate)  
Target: liquid H2 /  ${}^3\text{He}$   
Beam time: 3 shifts for beam-line re-commissioning  
12 shifts for calibration run with H2-target  
120 shifts for production run with  ${}^3\text{He}$ -target,  
corresponding to  $5 \times 10^{10}$  kaons on target

## 1 Summary of executed beam-time of the first-stage

The J-PARC E15 experiment [1] is aiming to investigate  $\bar{K}N$  interactions around the  $\bar{K}N$  threshold energy region via the in-flight  ${}^3\text{He}(K^-, n)$  reaction at 1 GeV/c, and searches for the simplest kaonic nuclear bound state, a  $K^-pp$  cluster [2, 3, 4]. As discussed at the previous PAC meetings, we have proposed to perform E15 stepwise. For the E15 first-stage, we requested beam-time corresponding to 30 kW·week integral primary-beam with Pt(Au) production-target. The first-stage experiment was successfully carried out in March and May, 2013, where  $1 \times 10^9$  and  $5 \times 10^9$  kaons were induced on  ${}^3\text{He}$  target, respectively. The beam-time of the first-stage is summarized in Table 1.

Table 1: Summary of the beam-time in the E15 first-stage run.

	Primary-beam intensity	Secondary-kaon intensity <sup>*1</sup>	Duration	Kaons on target <sup>*2</sup>
March, 2013 (Run#47)	14.5 kW (18 T <sub>ppp</sub> , 6s)	80 k/spill	30 h	$1.1 \times 10^9$
May, 2013 (Run#49c)	24 kW (30 T <sub>ppp</sub> , 6s)	140 k/spill	88 h	$5.1 \times 10^9$

<sup>\*1</sup> production target: Au 50% loss, spill length: 2s, spill duty factor:  $\sim 45\%$ , K/pi ratio:  $\sim 1/2$

<sup>\*2</sup> approximately 70% of beam kaons hit the fiducial volume of  $^3\text{He}$  target

## 2 Results and achievements of the first-stage

In spite of the limited beam time (2.5 + 12.5 kW·week), we succeeded in achieving the objectives of our first-stage run:

- (1) **obtain information on the  $\bar{K}N$  interaction via the  $^3\text{He}(K^-, n)$  spectrum below the  $\bar{K}NN$  threshold,**
- (2) **hunt a hint of the kaonic nuclear cluster in  $\Lambda + p + n$  final state,**
- (3) **investigate background processes, and**
- (4) **estimate realistic beam-time for the E15 full experiment.**

In this memorandum, we report results obtained by analysing the data accumulated in May, 2013. The results on each objective are described in the following sections.

### (1) $^3\text{He}(K^-, n)$ spectrum below the $\bar{K}NN$ threshold \*

Figure 1 shows the obtained  $1/\beta$  spectrum of neutral particles measured by a neutron counter array (NC), the analysed neutron momentum distribution, and the missing-mass spectrum of the  $^3\text{He}(K^-, n)$  reaction at  $\theta_{lab} = 0^\circ$ . Here, we required at least one charged track in a cylindrical detector system (CDS) that surrounds a liquid- $^3\text{He}$  target system to reconstruct reaction vertex. The spectrum is therefore distorted by the CDS acceptance of charged-track tagging. The spectrum shows a clear peak around  $2.4 \text{ GeV}/c^2$  which is attributed to the quasi-elastic  $K^-n \rightarrow K^-n$  and the charge exchange  $K^-p \rightarrow \bar{K}^0n$  reactions. In the binding region, substantial tail structure was observed having energy tail more than 100 MeV below the  $K^- + p + p$  energy threshold. As theoretical calculations shows [5, 6, 7], the sub-threshold structure is

---

\*This section is condensed from "Search for  $K^-pp$  bound state in the  $^3\text{He}(K^-, n)$  reaction at  $p(K^-) = 1 \text{ GeV}/c$ ", Tadashi Hashimoto, Ph.D. Thesis, The University of Tokyo, 2014.3.

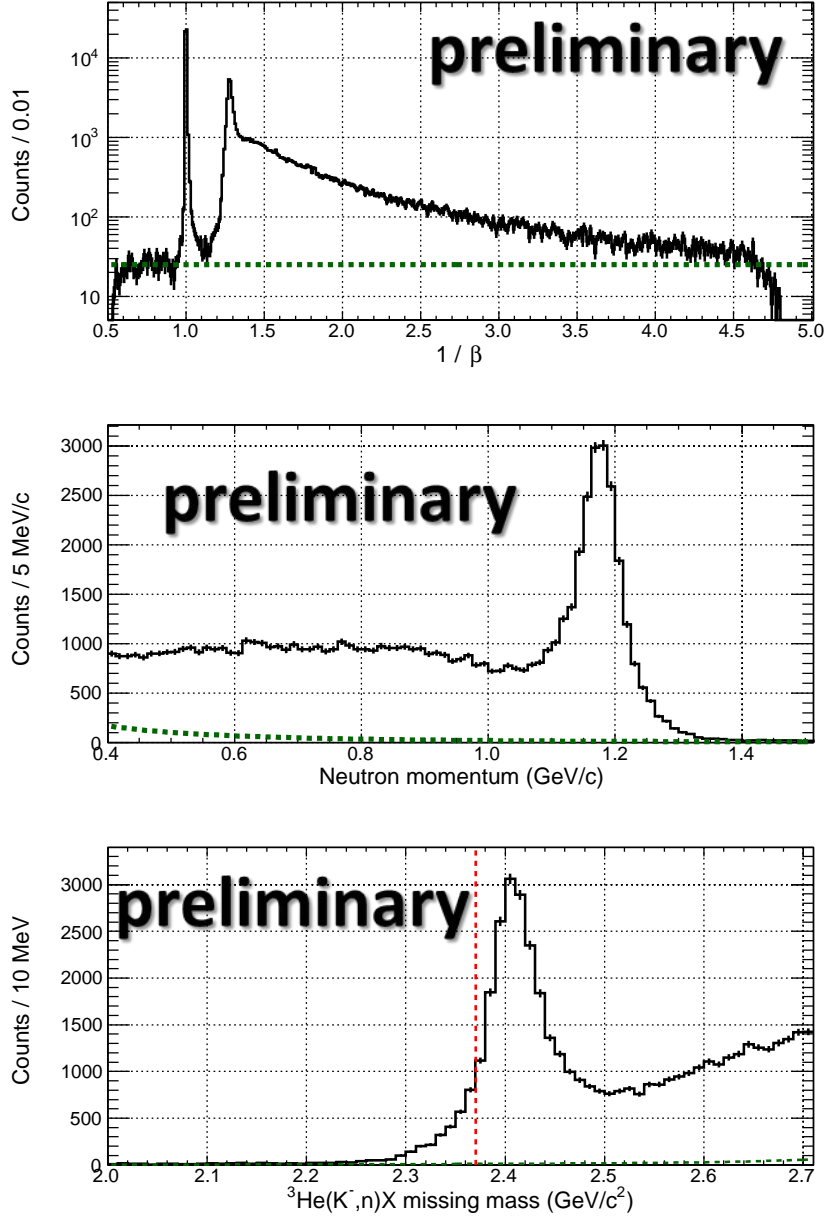


Figure 1: (top)  $1/\beta$  spectrum of neutral particles measured by the NC. The green dotted-line represents the accidental background evaluated by fitting the spectrum from 0.6 to 0.9 with a constant function. (middle) Neutron momentum distribution. (bottom)  ${}^3\text{He}(K^-, n)X$  missing-mass spectrum. The green dotted-line represents the accidental background converted from that in the  $1/\beta$  spectrum. The red dotted-line represents the  $K^-pp$  binding threshold.

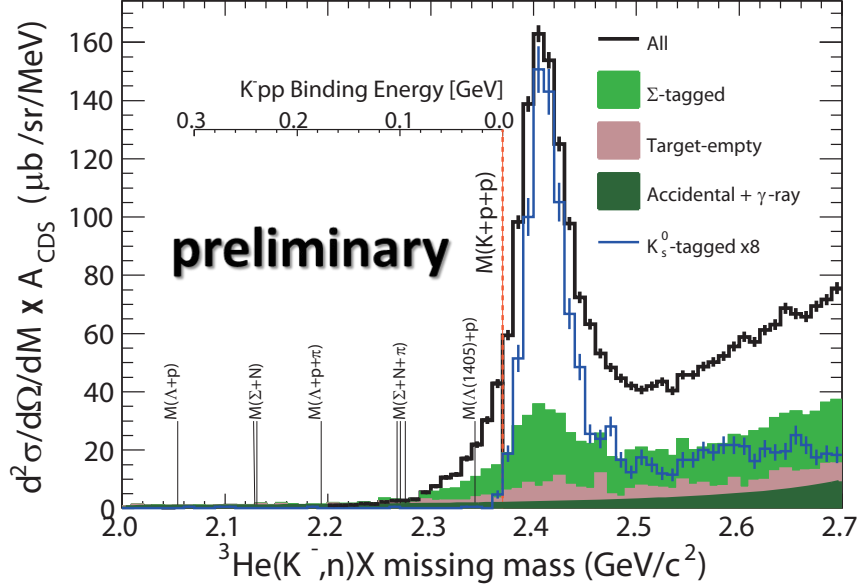


Figure 2: Normalized neutron missing-mass spectrum with the evaluated backgrounds. The blue histogram represents the  $K^0$ -tagged spectrum with a scale factor of 8. From the  $K^0$  tagged spectrum shape, the biggest structure above the  $K^-pp$  threshold comes from the kaon quasi-elastic reaction on one of the nucleon of  ${}^3\text{He}$  (Kaon quasi-free reaction).

quite sensitive to the  $\bar{K}N$  interaction and therefore the spectral shape largely depends on the interaction. To examine the sub-threshold structure in the obtained spectrum, we first evaluated backgrounds which are shown in Fig. 2. In the figure, cross-section of the spectrum was evaluated with integrated luminosity of  $540 \mu\text{b}^{-1}$ , NC acceptance of 22 msr, neutron detection efficiency of 0.23, and analysis efficiency of 0.68. It should be note that the systematic error of the neutron detection efficiency is evaluated as  $\pm 17\%$ , which is dominant contribution in the uncertainty for this measurement. Here we considered the following backgrounds in the region of interest:

- **Detector resolution**

The detector resolution can be evaluated from the edge-shape of the forward neutron spectrum at the  $K^-pp$  threshold, by requesting that the  $K^0$  is in the final state. In these events, high energy neutron can only be produced by the simple charge-exchange reaction,  $K^- {}^3\text{He} \rightarrow K^0 nd_s$ ; the  $K_S^0 \rightarrow \pi^+\pi^-$  decays can be reconstructed and identified by the CDS. In fact, the quasi-free spectrum, at around the  $K^-pp$  threshold energy, is well reproduced by a GEANT4[8]-based Monte Carlo simulation. The missing-mass resolution is evaluated to be  $\sim 10 \text{ MeV}/c^2$  ( $\sigma$ ) in the energy region of interest. Because of this excellent neutron energy res-

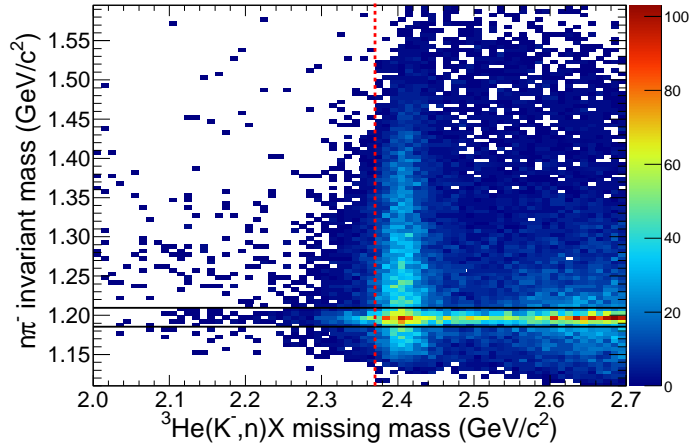


Figure 3: Correlation between the  $n\pi^-$  invariant mass and the neutron missing mass obtained from the experimental data. The mass region of  $\Sigma$ , indicated by thin black lines, was rejected from the semi-inclusive neutron spectrum. The red dotted-line represents the  $K^-pp$  binding threshold.

olution, contribution from the broadening of the quasi-free peak into the bound region is negligible.

- **Contamination from the material around the target**

We also evaluated contamination from the material around the target by analysing empty-target data. Because of the finite spatial resolution, the contamination events can survive even after the fiducial volume selection in the analysis, although the contamination is evaluated to be less than 10% of the  $^3\text{He}$  events in the bound region.

- **Accidental background and  $\gamma$ -ray contribution**

We need to consider two background sources, which could produce NC hit signals in between the  $\gamma$ -ray and the quasi-free peaks. One is accidental hits on the NC, which is coming randomly in time. This accidental background can be evaluated from the  $1/\beta$  spectrum in the unphysical region ( $1/\beta < 1$ ). The other is the tail component of the  $\gamma$ -ray peak, which is mainly coming from decay of  $\pi^0$  produced via secondary reactions. Both contributions can be evaluated from Fig. 1 (top), and the contribution of those backgrounds in the region of interest is evaluated to be less than 10% of the total yield below the  $K^-pp$  threshold.

- **Neutron contamination through  $Y$  decays**

Among kaon reactions with single nucleon, namely  $K^-N \rightarrow \pi Y$  elementary processes, only  $\Sigma^\pm$  productions can contribute to the background in the bound region through the reaction chain  $K^-N \rightarrow \pi\Sigma^\pm$  followed by  $\Sigma^\pm \rightarrow \pi^\pm n$ . Because

of the limited acceptance of the CDS in the backward direction, we are insensitive to the pion in the primary reaction when we require the forward neutron in the NC. Therefore, we are totally insensitive to  $K^-n \rightarrow \pi^-\Lambda$  followed by  $\Lambda \rightarrow \pi^0n$ . The remaining neutron backgrounds are from the  $\Sigma^\pm$  decays, however, we can efficiently reject those backgrounds event-by-event as shown in Fig. 3, by reconstructing  $\Sigma$  invariant-mass from the forward-going decay-neutron and the decay-pion detected by the NC and the CDS, respectively. The reconstruction efficiencies of the  $\Sigma^\pm$  decays are evaluated to be  $\sim 90\%$  by using the Monte Carlo simulation. Therefore, the neutron spectra after the  $\Sigma^\pm$ -decay neutron rejection is essentially free from hyperon decay backgrounds.

As shown in Fig. 2, the sub-threshold neutron yield cannot be reproduced by none of the well-known effects nor the processes listed above. After subtracting the  $\Sigma^\pm$ -decays event-by-event, we obtained the yields of the sub-threshold excess and that of the backgrounds as follows:

$$\begin{aligned} \text{excess :} & \quad 1731 \pm 41(\text{stat.}) \pm 193(\text{syst.}), \\ \text{backgrounds :} & \quad 467 \pm 40(\text{stat.}) \pm 73(\text{syst.}). \end{aligned}$$

The systematic errors are mainly due to uncertainty in the absolute scale of the missing mass evaluated to be  $\pm 3 \text{ MeV}/c^2$ . Thus, the origin of the sub-threshold excess should be attributed to the physical process, namely  $\bar{K}N$  interaction itself. In the following discussions, the  $\Sigma^\pm$ -decays subtracted neutron spectrum is used.

In general, sub-threshold excess can be explained by large imaginary part of the attractive  $\bar{K}N$  interaction. As a consequence, there could be following processes: two-nucleon absorption processes of  $K^-$  (2NA), three-nucleon absorption processes (3NA), and formation of a  $S = -1$  di-baryon state such as the  $K^-pp$  state. Because these processes are still not well studied both theoretically and experimentally, we compared the observed spectrum with expected ones evaluated by the Monte Carlo simulation based on simple s-wave PWIA interaction.

#### \* non-mesonic 2NA

Because there is a spectator nucleon in the final state, *i.e.*  $K^- {}^3\text{He} \rightarrow Y^{(*)}NN_S$  where  $N_S$  represent the spectator nucleon having the Fermi momentum of  ${}^3\text{He}$ , they are kinematically quasi two-body and highly energetic  $Y^{(*)}$  and  $N$  can be produced in rather narrow energy band as shown in Fig. 4. In the figure, simulated spectra of the non-mesonic 2NA are compared with the experimental semi-inclusive neutron spectrum assuming each process has equal cross section of 20 mb/sr in the forward direction.

As shown in the figure, the highest energy neutron (consequently the lowest missing mass) can be produced by the  $\Lambda N$  and the  $\Sigma N$  branches. Both primary neutrons and neutrons from hyperon decays locate at the deeply-bound region around  $2.1 \sim 2.2 \text{ GeV}/c^2$ , where there is no significant structure in the data.

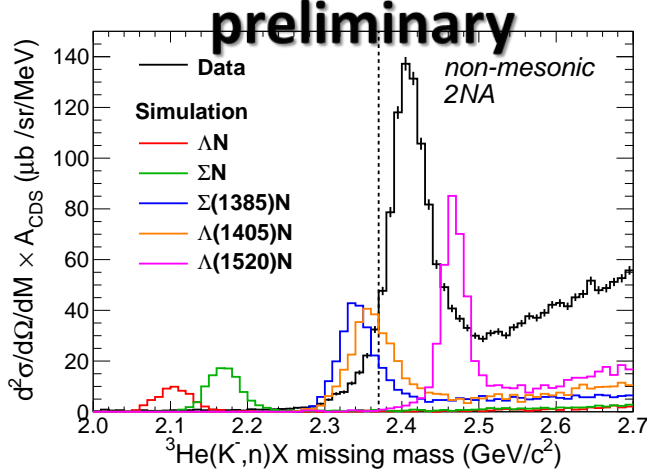


Figure 4: Comparison between the simulated neutron spectra of the non-mesonic 2NA and the observed  $\Sigma^\pm$ -subtracted spectrum. For each branch, the yield of 20 mb/sr at  $\theta_{lab} = 0^\circ$  is generated, where the relative reaction cross-section of each charge combination is assumed to be equivalent. The Breit-Wigner distributions with PDG masses and widths are used for resonance shapes of the hyperons.

We obtained an upper limit of the cross section to be  $\sim 0.3$  mb/sr. This is consistent with the result measured in  $^{12}\text{C}(K^-, N)$  reactions at 1 GeV/c by KEK PS-E548 [9].

We also examined  $Y^*$  contributions, in which neutron could be formed near the  $K^-pp$  energy threshold. Only from the semi-inclusive neutron spectrum, we cannot exclude the contribution of those process. To obtain the upper-limits of the cross sections of these branches, we performed pretty much simplified fitting to the semi-inclusive neutron spectra with the simulated  $Y^*N$  spectra (with  $Y^*$  mass and width fixed to the PDG values) and the  $K^0$ -tagged data; the  $K^0$ -tagged data will have almost identical spectral shape with the  $K^-N$  elastic reaction ( $K^-$  quasi-free). The result shows that one needs rather large cross-section of  $\sim 5$  mb/sr of  $\Lambda(1405)n$  branch to reproduce the observed sub-threshold excess.

#### \* mesonic 2NA and 3NA

Mesonic 2NA,  $K^- {}^3\text{He} \rightarrow \pi Y N N_S$ , and mesonic/non-mesonic 3NA,  $K^- {}^3\text{He} \rightarrow (\pi) Y N N$ , would produce broad continuums on the neutron missing mass spectrum as shown in Fig 5. In the figure, the simulated neutron spectra are generated unreasonably large cross-section of 100 mb each, so as to the spectral shape is visible. It is difficult to deduce all the related branching ratio to the individual charge states, but we can study rough branches categorized by the number of pions in the final state, assuming that the branch is similar to each possible

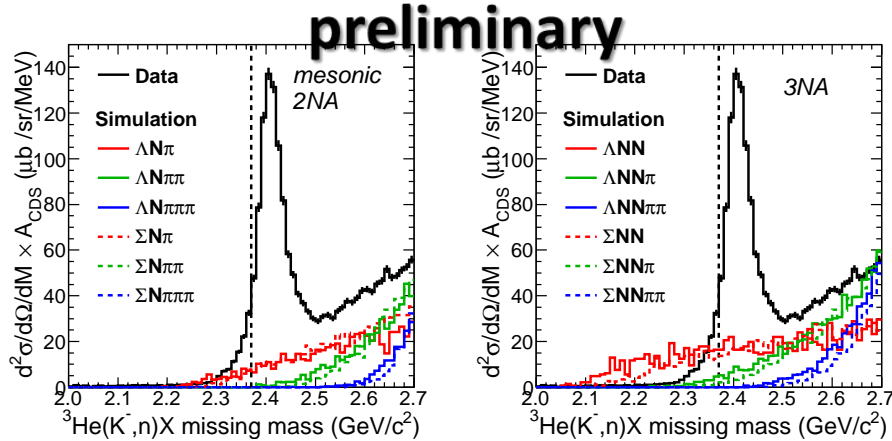


Figure 5: Simulated neutron spectra of (left) the mesonic 2NA and (right) the mesonic/non-mesonic 3NA with the observed  $\Sigma^\pm$ -subtracted spectrum. For each branch, the yield of 100 mb is generated, where the relative reaction cross section of each charge combination is assumed to be equivalent.

charge combinations by the kinematical analysis of  $\Lambda p$  pairs in the CDS<sup>†</sup>. From this analysis, the branches which can contribute to the bound region, including  $\Lambda N\pi$ ,  $\Sigma N\pi$ ,  $\Lambda NN$ ,  $\Sigma NN$ ,  $\Lambda NN\pi$  and  $\Sigma NN\pi$ , are evaluated to be less than 6 mb in total. Thus the contributions from these channels are much smaller than the sub-threshold excess. It should be noted that  $\Sigma - \Lambda$  conversion processes, *i.e.*  $K^- NN \rightarrow \Sigma N$  reactions followed by  $\Sigma N \rightarrow \Lambda N$  conversion with the spectator, have also small contribution in the bound region.

#### \* formation of the $K^- pp$ bound-state

In our semi-inclusive neutron spectrum, no clear peak structure was found at the energy much lower than the  $K^- pp$  threshold. The excess itself extends to the 100 MeV below the threshold, where FINUDA [10] and DISTO [11] with totally different reactions reported peak-like structure; they claimed the observation of the  $K^- pp$  state with (binding-energy, width) = (115, 67) and (103, 118) MeV in  $\Lambda p$  final state, respectively. We obtained upper limit of the formation cross section of the “deeply-bound  $K^- pp$  state” as shown in Fig. 6, which is evaluated by using the simple Breit-Wigner distribution as the spectral shape of the  $K^- pp$  state and  $K^- pp \rightarrow \Lambda p$  decay mode. The obtained upper limits for the FINUDA and the DISTO states are  $\sim 0.2$  and  $\sim 0.3$  mb/sr, respectively. Such small

<sup>†</sup>For example, in the missing mass spectrum of  ${}^3\text{He}(K^-, \Lambda p)X$  observed in the CDS (without requesting forward neutron hit in the NC), the mesonic 2NA channels open at  $m_n + N_\pi \times m_\pi$ , where  $N_\pi$  is the number of associated pions,  $m_n$  and  $m_\pi$  are the mass of neutron and that of pion, respectively (*c.f.* Fig. 7). Therefore, one can fit the data with the simulated spectra to deduce each yields.

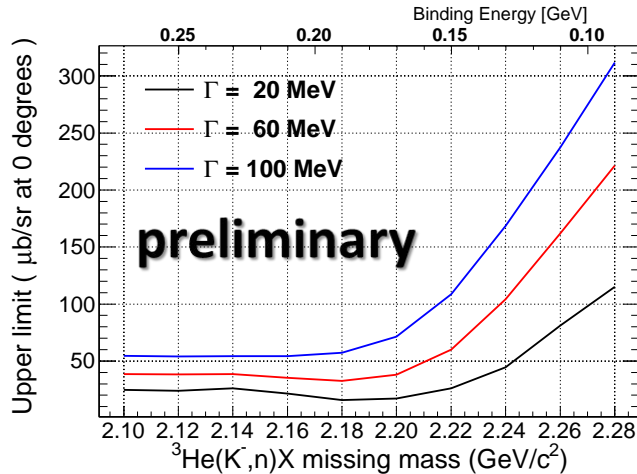


Figure 6: Upper limits of the formation differential cross-section at  $\theta_{lab} = 0^\circ$  for strange dibaryon state decaying into  $\Lambda p$  final state.

population cross section looks reasonable in view of the possible explanation of the observed sub-threshold excess by the  $\Lambda(1405) + n$  branch of 2NA with about 5 mb/sr, if the  $K^-pp$  bound state is formed through a  $\Lambda(1405) + p$  doorway sticking process.

At around the threshold, we have less sensitivity to the upper limit due to the excess below the threshold. In fact, one may attribute the excess to either it is formed by the “loosely-bound  $K^-pp$  state”, or it is caused by  $\Lambda(1405)N$  production via the non-mesonic 2NA as described above. Here we consider the former case, namely the excess is assumed to be fully originated from the “loosely-bound  $K^-pp$  state”. The differential cross-section at  $\theta_{lab} = 0^\circ$  is evaluated to be  $\sim 1$ mb/sr for each expected  $K^-pp$  decay mode of  $\Lambda p$ ,  $\Sigma^0 p$ , and  $(\pi\Sigma)^0 p$ . The obtained cross-section is similar to that of a theoretical calculation by Koike and Harada [5, 6]; they predicted the cross-section to be the order of mb/sr integrated in the bound region. Another theoretical group, Yamagata *et. al.*, also predicted the appearance of the sub-threshold structure in the in-flight  ${}^3\text{He}(K^-, n)$  spectrum [7]. They reported the sub-threshold cross-sections are one order of magnitude weaker than those of Koike and Harada’s calculation, however, the predicted cross-sections do not seem to be consistent with our results.

**In conclusion, no clear structure has been seen in the deeply bound region where FINUDA and DISTO observed the structure in different reactions, while the significant excess was observed around the  $\bar{K}NN$  threshold. To understand  $\bar{K}N$  interaction near the  $K^-pp$  threshold, exclusive measurements with higher statistics are inevitable.**

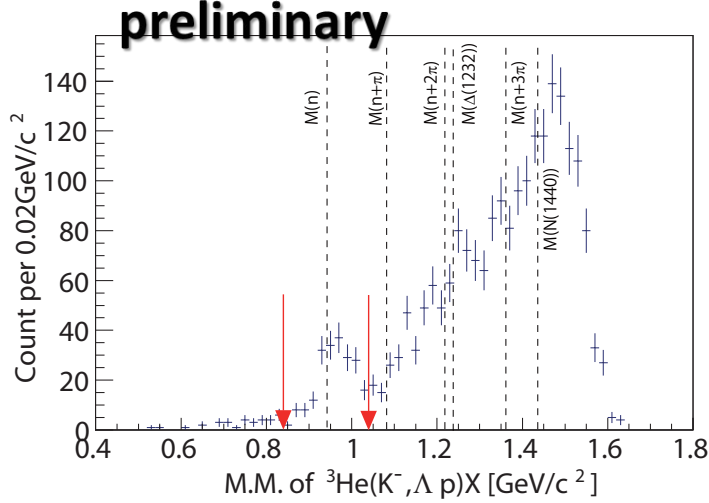


Figure 7: Missing mass of  ${}^3\text{He}(K^-, \Lambda p)X$ . The  $\Lambda pn$  events are selected in the region from 0.84 to 1.04  $\text{GeV}/c^2$  indicated by the arrows.

## (2) $\Lambda + p + n$ final state

The original objective of E15 is to perform exclusive analysis on the  ${}^3\text{He}(K^-, N)$  reaction, however, the available statistics in the first-stage does not allow us to perform full and redundant analysis both in formation and decay channels. Especially, the acceptance of the NC is quite limited, so let us start from  ${}^3\text{He}(K^-, \Lambda p)X$  channel. We reconstructed the  $\Lambda pn$  events by requiring a  $\Lambda p$  pair in the CDS and selecting a missing neutron in the  ${}^3\text{He}(K^-, \Lambda p)X$  missing-mass spectrum. Figure 7 shows the missing-mass of  ${}^3\text{He}(K^-, \Lambda p)X$ , which has a clear peak at  $M(X) = M(n)$ . As it is shown, multi- $\pi$  formation events are clearly separated from the missing-neutron peak. By selecting the missing neutron mass region from 0.84 to 1.04  $\text{GeV}/c^2$ , about 190  $\Lambda pn$  events were identified. Note that we cannot exclude  ${}^3\text{He}(K^-, \Sigma^0 p)n$  events from this event selection due to the limited CDS resolution. We evaluated the  $\Sigma^0$  yield to be  $\sim 20\%$  in the selected  $\Lambda pn$  events by fitting the missing-mass of  ${}^3\text{He}(K^-, \Lambda p)X$  spectrum with the expected spectra obtained by the Monte Carlo simulation.

Then, Dalitz plot of  $\Lambda pn$  in the CM frame is obtained as shown in Fig. 8 (left). We found that the selected  $\Lambda pn(\Sigma^0 pn)$  events are widely distributed over the kinematically-allowed phase-space indicated by black circle. We are insensitive to the region of upper left and upper right corner of the boundary, because kinetic energies of  $p$  and  $\Lambda$  (consequently  $p\pi^-$ -pair) are too small to escape from the target.

It is quite interesting that very few events can be seen in the bottom of the boundary, where the non-mesonic 2NA events of  $K^- {}^3\text{He} \rightarrow \Lambda pn_S$  are expected. Moreover, there is no clear signal of cascade reaction chain involving a spectator “neutron” after the primary non-mesonic 2NA processes. Another interesting point is that the event distribution is rather uniform over the kinematically allowed region. Such events can

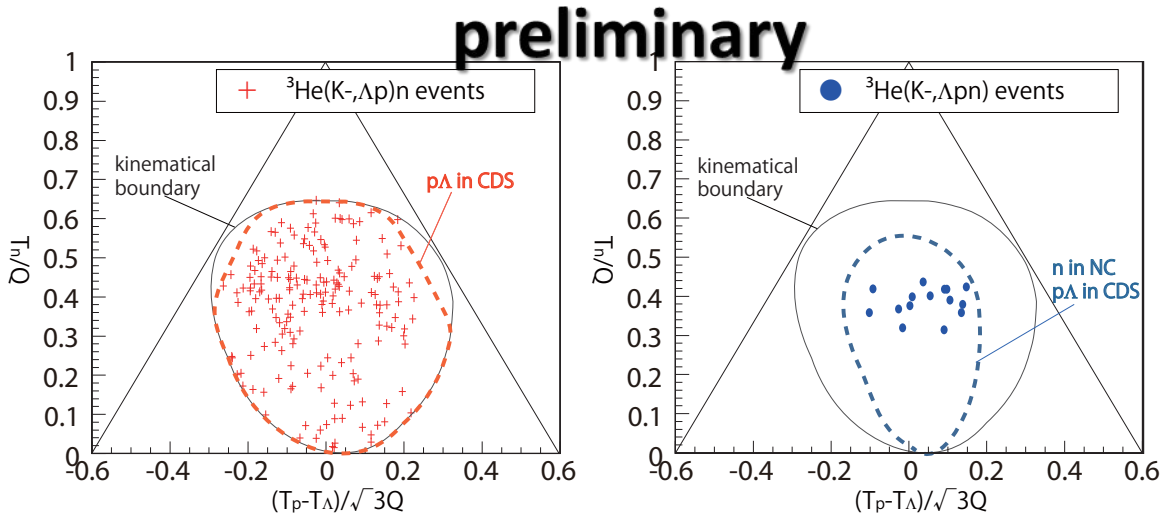


Figure 8: (left) Dalitz plot of  $\Lambda pn$  in the exclusive  ${}^3\text{He}(K^-, \Lambda p)n$  events whose neutron is selected by the  ${}^3\text{He}(K^-, \Lambda p)X$  missing mass. (right) If the neutron detection by the NC is required, only 15 events are left. The area surrounded by dotted line show the detector acceptances. The vertical axis is normalized neutron kinetic energy in CM frame, and the horizontal axis is normalized energy difference between proton and  $\Lambda$ , where  $Q$  is the  $Q$ -value of the reaction.

only be produced in the 3NA reaction. It is also interesting to note that the thick event band can be seen having similar neutron kinetic energy. If the  $\Lambda pn$  events are originated from the  $K^-pp$  formation, such events would appear as strong correlations in the Dalitz plot with similar neutron kinetic energy. One might expect that the non-mesonic 2NA  $\Sigma$  production, followed by  $\Sigma$ - $\Lambda$  conversion on a spectator nucleon, would produce similar band structure. However, it is not likely because 1) the non-mesonic 2NA processes seem to be weak, and 2) no other cascade process can be seen.

To study full-kinematically-resolved events, we plotted the forward-neutron detected events in Fig. 8 (right). As shown in the figure, NC hit events locate only close to the thick band observed in Fig. 8 (left).

Figure 9 shows the invariant mass, the opening angle, and the momentum distributions for the experimental data shown in Fig. 8 (left) together with the phase-space based simulations. The  $\Lambda p$  invariant mass of the exclusive channel of  ${}^3\text{He}(K^-, \Lambda p)n_{\text{missing}}$  is shown in Fig 9 (A), in which events distribute from  $2.05 \text{ GeV}/c^2$  ( $=M(\Lambda + p)$  kinematic boundary) to  $2.9 \text{ GeV}/c^2$ . As shown in the figure, background due to the  $\Lambda$  miss-identification is quite small. The thick band, observed in the Dalitz plot, corresponds to the structure seen close to the  $K^-pp$  threshold. Except for this region, the global structure can be explained by two possible 3NA processes. It should be noted that the spectrum can be compared to the semi-inclusive  ${}^3\text{He}(K^-, n)X$  channel given in Fig. 2. This structure seen close to the threshold cannot be attributed to the  $\Lambda(1405)n$  processes as a possible interpretation account for the sub-threshold excess

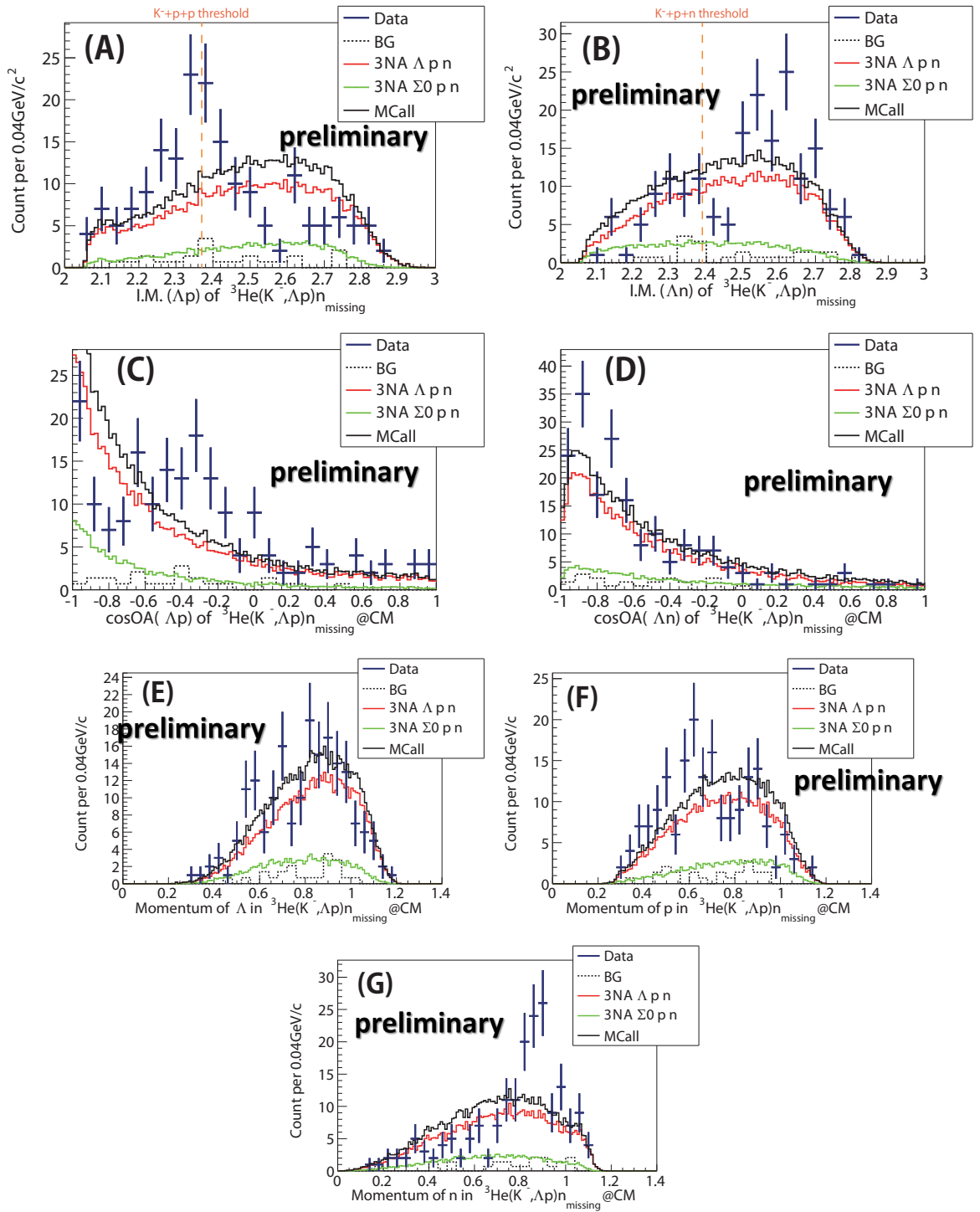


Figure 9: (A,B) Invariant mass, (C,D) opening angle, and (E,F,G) momentum distributions of the exclusive  ${}^3\text{He}(K^-, \Lambda p)n$  events. The experimental data and the phase-space simulations are compared within the E15 acceptance. The yield of the simulated spectra is normalized to the data, where the relative yield of each simulated spectrum is evaluated by fitting the missing-mass spectrum of  ${}^3\text{He}(K^-, \Lambda p)X$  with the simulated spectra.

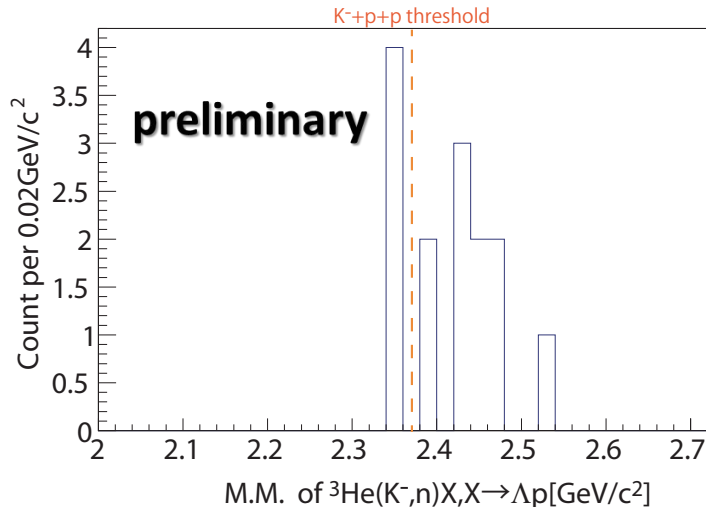


Figure 10: Neutron spectrum at  $\theta_{lab} = 0^\circ$  with the kinematically-complete measurement of  ${}^3\text{He}(K^-, \Lambda pn)$ .

in Fig. 2. As it is expected, quasi-elastic channels are almost completely suppressed in  $\Lambda pn$  final state. Figure 9 (B) shows the  $\Lambda n$  invariant mass spectrum. No clear structure can be seen in this spectrum.

In the opening angle between  $\Lambda$  and  $p$  shown in Fig. 9 (C), excess from the 3NA processes can be seen in the region from -0.5 to -0.2. This is quite interesting because the opening angle of  $\Lambda p$  decay from a  $S = -1$  di-baryon state is expected to distribute around this region when the mass of the state is around the  $K^-pp$  threshold. Note that, in the in-flight reaction of  $K^-+{}^3\text{He}$ ,  $\Lambda p$  decay from a  $S = -1$  di-baryon state is not back-to-back in the CM frame, in contrast to the stopped  $K^-$  reaction. Figure 9 (G) shows the momentum distribution of the missing neutron, where excess around 0.9 GeV/ $c$  corresponds to the thick band in the Dalitz plot.

**In conclusion, structure around the  $K^-pp$  threshold ( $\sim 2370$  MeV/ $c^2$ ) can be seen in the  $\Lambda p$  invariant-mass spectrum over the wide distribution coming from the 3NA processes, whereas no strong event structure was found at around  $\sim 2270$  MeV/ $c^2$  revealed in the  $\Lambda p$  invariant-mass in  $K^-$  capture by FINUDA and in the  $pp \rightarrow \Lambda p K^+$  reaction at DISTO. To investigate the  $\Lambda pn$  distribution more clearly, it is necessary to carry out high statistics experiment.**

— neutron spectrum at  $\theta_{lab} = 0^\circ$  with the  ${}^3\text{He}(K^-, \Lambda pn)$  measurement —

One of the final goal of the E15 experiment is to observe the nature of the  $K^-pp$  state via the kinematically-complete  ${}^3\text{He}(K^-, \Lambda pn)$  measurement. Although the detector acceptance for the  ${}^3\text{He}(K^-, \Lambda pn)$  measurement is very limited, the minimum

momentum transfer of  ${}^3\text{He}(K^-, n)X$  reaction is realized by the forward neutron measurement, which would enhance the formation of the strange di-baryon. Therefore, it is worthwhile to demonstrate the neutron spectrum at  $\theta_{lab} = 0^\circ$  with the  ${}^3\text{He}(K^-, \Lambda pn)$  measurement using the first-stage data. Figure 10 shows the obtained neutron spectrum at  $\theta_{lab} = 0^\circ$  for the same event set shown in Fig.8 (right). The ratio of events between below and above the threshold are different from semi-inclusive neutron spectrum, although, we do not have enough statistics to have definitive interpretation. To know the structure near threshold with full-kinematically-resolved event set, we need much more data.

### (3) background study

As already discussed in the  ${}^3\text{He}(K^-, n)$  and  ${}^3\text{He}(K^-, \Lambda p)n$  analyses, the background studies were performed. A summary is listed as follows:

- The accidental background in the  $(K^-, n)$  measurement was kept at low level; the signal to noise ratio at the quasi-free peak was achieved to be more than 100. The background coming from materials other than  ${}^3\text{He}$  target was also under control.
- It was confirmed that neutron background from  $K^-N \rightarrow \pi\Sigma^\pm$  reaction followed by  $\Sigma^\pm$  decays can be safely eliminated from the semi-inclusive neutron spectrum event-by-event.
- The non-mesonic two-nucleon absorption processes of  $K^-NN \rightarrow \Lambda N/\Sigma N$  branches were found to be negligibly small in the in-flight  ${}^3\text{He}(K^-, n)$  reaction at 1 GeV/c.
- In the region below the  $K^-+p+p$  threshold of the  ${}^3\text{He}(K^-, n)$  spectrum, contribution from the mesonic two-nucleon and the mesonic/non-mesonic three-nucleon absorption processes were evaluated to be negligible, although such processes could be main background processes for the observed sub-threshold excess.
- The events of  $\Lambda(\Sigma^0)pn$  final state seem to be widely distributed over the phase-space. No strong correlations originating from the two-nucleon absorption processes were observed.

### (4) beam-time estimation

In the first-stage experiment,  $6 \times 10^9$  kaons were induced on  ${}^3\text{He}$  target which corresponds to  $\sim 1\%$  of the approved proposal. With the data sample of  $5 \times 10^9$  incident kaons, we obtained the yields of:

- semi-inclusive  ${}^3\text{He}(K^-, n)$ :  $\sim 2200$  events in the sub-threshold region,
- exclusive  ${}^3\text{He}(K^-, \Lambda p)n$ :  $\sim 190$  events, and
- exclusive  ${}^3\text{He}(K^-, \Lambda pn)$ :  $\sim 15$  events.

To accomplish the E15 experiment with the kinematically-complete measurement of  ${}^3\text{He}(K^-, \Lambda pn)$ , we estimate that more than 100 times incident kaons are required.

**Thus, the goal of the first-stage experiment was successfully achieved, and hints about strange di-baryon (or “ $K^-pp$ ” state in short) were obtained. To investigate exclusive channels and to understand the  $K^-N$  interaction in detail, we proceed to the second-stage experiment before the full E15.** The results of the semi-inclusive  ${}^3\text{He}(K^-, n)$  and the exclusive  ${}^3\text{He}(K^-, \Lambda p)n$  analyses will be finalized and published soon. In addition,  ${}^3\text{He}(K^-, p)$  analysis is also ongoing to investigate the iso-spin dependence of the kaon-nucleus ( $\bar{K} - NN$ ) interaction.

Finally, research output of E15 up to now (2007 - 2014) is summarized in Table .2. Moreover, we expect three more PhD theses and four more physics papers will appear within a year.

Table 2: Summary of research output of E15 (2007 - 2014).

Thesis	doctor	1
	master	5
Publication	technical paper	3
	conference proceedings	15
Public presentation	international	25
	national	33

### 3 Conclusion of the fist-stage physics run

We carried out the E15 first-stage run in March and May, 2013. The goal of the first-stage was successfully accomplished, and the significant excess around the  $\bar{K}NN$  threshold was observed both in the neutron missing-mass and the  $\Lambda p$  invariant-mass spectra. The obtained results have already given us some hints about the nature of the  $K^-pp$  bound-state and of the  $\bar{K}N$  interaction. To investigate the obtained hints in detail, we require the next beam-time for the second-stage E15 data-taking run.

### 4 Request of the second-stage beam-time

As discussed in the previous section, we request more than 100 times beam-time than that of the first-stage to complete the E15 full experiment. This is almost equivalent to our requested beam-time in the approved proposal: full PS intensity of  $9 \mu\text{A}$  proton at

30 GeV (270kW) for 5.5 weeks corresponding to  $\sim 1$  MW·week. However, 1 MW·week production run seems to be hard to be realized in short term at present.

On the other hand, over recent years, impressive progresses of the kaonic-nuclei study have been made both in theoretical and experimental works. In particular, experimental studies by HADES [12], SPring-8/LEPS [13], J-PARC E27 [14], and our experiment E15 have given new insight of the  $K^-pp$  state which would be significant hints of the  $\bar{K}N$  interaction around the threshold-energy region. Among the experiments, the kaon-induced experiment, *i.e.* E15, is unique and therefore would provide unique experimental information because the simplest reaction of  ${}^3\text{He}(K^-, n)$  at 1 GeV/ $c$  has been used as experimental technique.

Therefore, to address all the possible information about the  $\bar{K}N$  interaction with present beam-power of the MR, we would like to perform a second-stage production run of E15 with  $50 \times 10^9$  kaons on target, which corresponds to 10 times larger statistics than that of the first-stage run in May, 2013. In the second-stage, we aim to:

- (1) **confirm the spectral shape of the  $\Lambda p$  invariant-mass by the exclusive measurement of  ${}^3\text{He}(K^-, \Lambda p)n$ , and**
- (2) **explore the neutron spectrum at  $\theta_{lab} = 0^\circ$  with the kinematically-complete measurement of  ${}^3\text{He}(K^-, \Lambda pn)$ .**

In the previous run in May, 2013 (RUN#49c), the  $K^-$  intensity of  $\sim 140$  k/spill was obtained with  $\sim 0.5$   $K/\pi$  ratio at 24 kW MR-power (30 Tppp, 6s repetition, 2s spill length). Based on the kaon yield above, we would request the following beam-time as the E15 second-stage run:

**1. 1-day for the K1.8BR beam-line re-commissioning:**

We need to perform re-commissioning of the  $K^-$  beam once again to confirm the beam quality, since production-target configuration, primary-beam orbit, and beam-line apparatuses around production-target were changed due to safety reasons.

**2. 4-days for calibration run with H2 target:**

This is a leftover from the first-stage run, which was scheduled to be performed in May, 2013. The aim of this run is to evaluate the neutron detection-efficiency of the NC using the charge-exchange reaction  $K^-p \rightarrow K^0n^\ddagger$ . Reconstruction of the  $K_S^0 \rightarrow \pi^+\pi^-$  decay by the CDS enables us to obtain the exact neutron-kinematics, thus we can precisely evaluate the neutron detection-efficiency. The expected yield of the  $p(K^-, K^0)n$  events is  $\sim 1 \times 10^4$ , where we can determine the detection efficiency with  $\sim 1\%$  accuracy. Note that confirmations of the detector effects in the  $(K^-, n)$  spectrum and the elementary  $K^-p$  reactions are also performed.

---

<sup>‡</sup>Indeed, the neutron detection-efficiency was obtained with  ${}^3\text{He}$  target using this method, however, large uncertainty of the efficiency remained due to the Fermi motion of nucleons in  ${}^3\text{He}$ .

### 3. 40-days for production run with $^3\text{He}$ target:

We carry out the second-stage production run of E15 with  $50 \times 10^9$  kaons on target, which corresponds to 10 times larger statistics than that of the first-stage run in May, 2013. In the second-stage run, we expect to obtain (1)  $\sim 2000$  and (2)  $\sim 150$  events of  $^3\text{He}(K^-, \Lambda p)n$  and  $^3\text{He}(K^-, \Lambda pn)$ , respectively. With the data-sample, we perform detailed investigation whether the observed excess is originated from a  $S = -1$  dibaryon, such as the  $K^-pp$  state, or not.

## References

- [1] M. Iwasaki *et al.*, J-PARC E15 proposal,  
[http://j-parc.jp/NuclPart/pac\\_0606/pdf/p15-Iwasaki.pdf](http://j-parc.jp/NuclPart/pac_0606/pdf/p15-Iwasaki.pdf).
- [2] Y. Akaishi and T. Yamazaki, Phys. Rev. C **65**, 044005 (2002).
- [3] T. Yamazaki and Y. Akaishi, Phys. Lett. B **535**, 70 (2002).
- [4] T. Yamazaki and Y. Akaishi, Phys. Rev. C **76**, 045201 (2007).
- [5] T. Koike and T. Harada, Phys. Lett. B **652** (2007) 262.
- [6] T. Koike and T. Harada, Phys. Rev. C **80** (2009) 055208.
- [7] J. Yamagata-Sekihara, D. Jido, H. Nagahiro and S. Hirenzaki, Phys. Rev. C **80** (2009) 045204.
- [8] S. Agostinelli *et al.*, Nucl. Instr. and Meth. **A506** (2003) 250.
- [9] T. Kishimoto *et al.*, PTP, **118** (2007) 181.
- [10] M. Agnello *et al.*, Phys. Rev. Lett. **94** (2005) 212303.
- [11] T. Yamazaki *et al.*, Phys. Rev. Lett. **104** (2010) 132502.
- [12] L. Fabbietti *et al.*, Nucl. Phys. A **914** (2013) 60.
- [13] A. O. Tokiyasu, Phys. Lett. B **728** (2014) 616.
- [14] presentation on J-PARC 17th PAC.